Version of record at: https://doi.org/10.1063/5.0278907

RESEARCH ARTICLE | NOVEMBER 19 2025

Energy transfer and conversion in magnetic reconnection: Observation and simulation

S. Roy ; R. Bandyopadhyay ; S. Adhikari ; Y. Yang ; W. H. Matthaeus

Phys. Plasmas 32, 112302 (2025)
https://doi.org/10.1063/5.0278907
CHORUS

Physics of Plasmas ARTICLE pubs.aip.org/aip/pop

Energy transfer and conversion in magnetic reconnection: Observation and simulation

Cite as: Phys. Plasmas **32**, 112302 (2025); doi: 10.1063/5.0278907
Submitted: 4 May 2025 · Accepted: 21 October 2025 ·
Published Online: 19 November 2025

View Online Export Citation CrossMark

S. Roy,[1] R. Bandyopadhyay,[1,2,a)] S. Adhikari,[1] Y. Yang,[1] and W. H. Matthaeus[1]

AFFILIATIONS

[1]Department of Physics and Astronomy, University of Delaware, Newark, Delaware 19716, USA
[2]Department of Astrophysical Sciences, Princeton University, Princeton, New Jersey 08544, USA

[a)]Author to whom correspondence should be addressed: riddhib@udel.edu

ABSTRACT

One of the central problems in collisionless plasma turbulence is to understand the nature of the cross-scale energy transfer and dissipation occurring at kinetic scales. Magnetic reconnection plays an important role in dissipating energy and driving energy transfer in these systems. However, for reconnection, a detailed picture of the fluxes of energy in its several forms, and the conversion among them, until now remains unclear. In this study, a scale filtering method is adopted to explore how energy is converted between different forms and transferred across scales in turbulent magnetic reconnection using a combination of Magnetospheric Multiscale observations and particle-in-cell simulations. Two novel findings of this paper are that both ion and electron dissipation start to occur at sub-ion scale, at nearly same scale, and that most of the energy cascade due to reconnection is carried by the electron fluid.

I. INTRODUCTION

In the standard picture of hydrodynamic turbulence, energy is injected at the largest scales, which then cascades down the inertial range, and is finally lost to random motions of the particles in the dissipation range.[1] This picture has been extended to magnetohydrodynamics (MHD) and plasma turbulence, but the mechanisms through which energy dissipation and transfer occur as well as the nature of the energy cascade are not very well understood.[2–4] Using both fluid and kinetic models, significant progress has been made in understanding plasma turbulence using spectral analysis, structure functions, and scale decomposition.[5–8] Extending these studies and techniques to the particular case of magnetic reconnection remains at an early stage—see, however, Refs. 9 and 10. Here, we advance the study of reconnection by applying scale filtering methods to energy transfer and an exact representation of collisionless dissipation.

Magnetic reconnection is a fundamental plasma process that involves topological change of magnetic field lines, leading to conversion of magnetic energy to kinetic energy. Large-scale reconnection can trigger turbulence cascade,[11] and small-scale reconnection naturally occurs at thin current sheets in a turbulent plasma.[12–14] The interplay of turbulence and reconnection is an active field of research.[15–19] Observations of spectra of turbulent electromagnetic fluctuations have revealed the presence of a break near the ion inertial scale,[20] a scale at which the ions become decoupled from the electrons. It has been proposed that magnetic reconnection plays an important role in driving the energy transfer at these sub-ion scales.[21] Indeed, recent studies[10,22] have conclusively demonstrated that magnetic reconnection drives sub-ion scale energy transfer in collisionless plasmas. At the same time, reconnecting current sheets was shown to be sites of enhanced dissipation or conversion of energy.[23,24] The present operative definition of "dissipation" is based on the identification of the species dependent pressure-strain interactions as the channels for the conversion of flow energies into internal energies.[8,23] It is worth noting that other definitions of dissipation have also been proposed such as those based on irreversible energy conversion,[25] irreversible production of entropy,[26,27] and distortion of the distribution function[28] (see Pezzi *et al.*[29] for a review). Other processes such as electromagnetic work and heat flux are also of prime importance in tracking energy transport and conversion in collisionless plasma. However, the detailed interaction of these processes has not been fully studied in the context of reconnection, especially when interactions are decomposed according to scale using filtering methods.[8,30] In this paper, we examine every component of energy transfer and conversion, each decomposed across scale using filtering, within identified diffusion regions of magnetic reconnection in both simulations and MMS observations.

II. THEORY

To disentangle the dynamics of a turbulent field $\mathbf{u}$, one can adopt a filtering approach[31,32] and describe the field filtered on a length scale ℓ and time scale τ as

$$\overline{u_i(\mathbf{x},t)}_{\ell,\tau} = \int u_i(\mathbf{x}',t')\mathcal{G}(\mathbf{x}-\mathbf{x}',t-t';\ell,\tau)\,\mathrm{d}^3\mathbf{x}'\mathrm{d}t', \tag{1}$$

where $\mathcal{G}$ is a normalized filtering kernel following

$$\int \mathcal{G}(\mathbf{x}-\mathbf{x}',t-t';\ell,\tau)\mathrm{d}^3x'\mathrm{d}t' = 1. \tag{2}$$

In spacecraft observations, since we only have access to a one-dimensional time series, our filtering Eq. (1) simplifies to

$$\overline{u_i(t)}_{\tau} = \int u_i(t')\mathcal{G}(t-t';\tau)\,\mathrm{d}t'. \tag{3}$$

The simplest filter one can use is the boxcar filter

$$\overline{u_i(t)}_{\tau} = \frac{1}{\tau}\int_t^{t+\tau} u_i(t')\,\mathrm{d}t'. \tag{4}$$

We have used the Taylor's frozen-in hypothesis[33] in interpreting time series data as a one-dimensional spatial sample. For reconnection events in particular, which are known to be inhomogeneous and non-stationary, this conversion to spatial lags may be viewed as questionable in some circumstances. An example would be if an event is dominated by high phase velocity dynamics such as whistlers. We proceed with caution, and the caveat that the true filter operation is in time and the interpretation as filtering in space is approximate.

In addition, it is often found convenient to introduce a different filtering operation, known as *Favre* filtering,[34] which takes the density ρ into account, and for any physical quantity f, it is defined by $\widetilde{f} = \overline{\rho f}/\overline{\rho}$. The Favre filtering becomes important when there are large density variations in the flow, or the flow is compressible. This can lead to different ways of defining the dissipation function, as we find in Refs. 30 and 35. A brief discussion of the discrepancies is found in Appendix.

For completeness, we briefly discuss here the steps involved in deriving the scale-filtered Vlasov–Maxwell equations. The Vlasov equation for each of the one-body particle distribution functions f_α for species α is given by

$$\partial_t f_\alpha + \mathbf{v}\cdot\nabla f_\alpha + \frac{q_\alpha}{m_\alpha}\nabla_{\mathbf{v}}\cdot\left[\left(\mathbf{E}+\frac{\mathbf{v}}{c}\times\mathbf{B}\right)f_\alpha\right] = 0. \tag{5}$$

The filtering operation as described in Eq. (1) is then applied to each term in the Vlasov equation (5), and using the fact that the filtering operation commutes with temporal and spatial derivatives, we can write

$$\partial_t\overline{f}_\alpha + \mathbf{v}\cdot\nabla\overline{f}_\alpha + \frac{q_\alpha}{m_\alpha}\nabla_{\mathbf{v}}\cdot\left[\overline{\mathbf{E}f_\alpha} + \frac{\mathbf{v}}{c}\times\overline{\mathbf{B}f_\alpha}\right] = 0. \tag{6}$$

The second moments of these filtered equations are then given by[3,8,35,36]

$$\partial_t\mathcal{E}^{f,<}_\alpha + \nabla\cdot\mathbf{J}^u_\alpha = -\Pi^{uu}_\alpha - PS^<_\alpha + W^<_\alpha. \tag{7}$$

Similarly, one can apply the filtering operation on the equation for the time evolution of the electromagnetic energy,

$$\partial_t\mathcal{E}^{m,<} + \nabla\cdot\mathbf{J}^b = -\sum_\alpha\Pi^{bb}_\alpha - \sum_\alpha W^<_\alpha. \tag{8}$$

In the aforementioned equations and the following equations, the superscript $<$ is referring to the low-pass filtering operation described in Eqs. (3) and (4). Here, $\mathcal{E}^{f,<}_\alpha = \frac{1}{2}\overline{\rho}_\alpha\widetilde{\mathbf{u}}^2_\alpha$ is the filtered fluid flow energy of charged species α, and $\mathcal{E}^{m,<} = (\overline{\mathbf{B}}^2+\overline{\mathbf{E}}^2)/(8\pi)$ is the filtered electromagnetic energy. $\mathbf{J}^u_\alpha = \mathcal{E}^{f,<}_\alpha\widetilde{\mathbf{u}}_\alpha + \overline{\rho}_\alpha\widetilde{\boldsymbol{\tau}}^u_\alpha\cdot\widetilde{\mathbf{u}}_\alpha + \overline{\mathbf{P}}_\alpha\cdot\widetilde{\mathbf{u}}_\alpha$ and $\mathbf{J}^b = (c\overline{\mathbf{E}}\times\overline{\mathbf{B}})/4\pi$ are the filtered spatial transport terms corresponding to the kinetic and electromagnetic energies, respectively. The filtering operation also produces two additional terms, which are not present in the unfiltered moment equations. These are Π^{uu}_α and Π^{bb}_α, describing the scale-to-scale transfer of the kinetic and electromagnetic energies, respectively. We define these terms as follows:

$$\Pi^{uu}_\alpha = -(\overline{\rho}_\alpha\widetilde{\boldsymbol{\tau}}^u_\alpha\cdot\nabla)\cdot\widetilde{\mathbf{u}}_\alpha - \frac{q_\alpha}{c}\overline{n}_\alpha\widetilde{\boldsymbol{\tau}}^b_\alpha\cdot\widetilde{\mathbf{u}}_\alpha \tag{9}$$

is the flux of large-scale fluid flow energy transferred to sub-scale fluid flow energy, with $\widetilde{\boldsymbol{\tau}}^u_\alpha = \widetilde{\mathbf{u}_\alpha\mathbf{u}_\alpha} - \widetilde{\mathbf{u}}_\alpha\widetilde{\mathbf{u}}_\alpha$ and $\widetilde{\boldsymbol{\tau}}^b_\alpha = \widetilde{\mathbf{u}_\alpha\times\mathbf{B}} - \widetilde{\mathbf{u}}_\alpha\times\widetilde{\mathbf{B}}$ being the subgrid scale Reynolds stress and the turbulent emf (electromotive force), respectively. $W^<_\alpha = q_\alpha\overline{n}_\alpha\widetilde{\mathbf{E}}_\alpha\cdot\widetilde{\mathbf{u}}_\alpha$ is the rate of fluid flow energy converted into electromagnetic energy at sub-scale due to larger scale interactions. Similarly,

$$\Pi^{bb}_\alpha = -q_\alpha\overline{n}_\alpha\widetilde{\boldsymbol{\tau}}^e_\alpha\cdot\widetilde{\mathbf{u}}_\alpha \tag{10}$$

is the flux of electromagnetic energy from large scales due to the work done by the sub-scale electric field $\widetilde{\boldsymbol{\tau}}^e_\alpha = \widetilde{\mathbf{E}} - \overline{\mathbf{E}}$, and finally,

$$PS^<_\alpha = -(\overline{\mathbf{P}}_\alpha\cdot\nabla)\cdot\widetilde{\mathbf{u}}_\alpha \tag{11}$$

is the rate of low frequency fluid flow energy converted into thermal energy at smaller scales.

III. MMS OBSERVATIONS

We apply the scale filtering technique to study a symmetric reconnection event in the magnetosheath observed by Magnetospheric Multiscale (MMS)[38] Mission. In this event, the guide field was approximately half of the reconnecting magnetic field. MMS observed an electron jet, which was skewed toward the separatrix, consistent with previous simulations of reconnection with a moderate guide field. This was accompanied by a clear spike in $\mathbf{j}\cdot\mathbf{E}'$, indicating conversion of electromagnetic energy into kinetic energy of the plasma. For more details of this event, please see Wilder *et al.*[37] The magnetic shear angle across the current sheet was computed to be $\sim 136°$. The ion and electron densities are found to be roughly constant throughout this event, at around $20\,\mathrm{cm}^{-3}$. The average proton and electron beta during the event are found to be 5.5 and 1.2, respectively. The ion jet in this event is unclear, which might indicate that this is an early stage of an ion-coupled reconnection event. An overview of this event is given in Fig. 1, which shows the magnetic field in GSE (Geocentric Solar Ecliptic) coordinates[39] as well as the ion and electron velocities. The vertical dotted lines in the figure indicate the observed electron diffusion region, also known as the EDR. The availability of multi-spacecraft measurements from MMS enables us to compute gradients of ion and electron velocities, which are essential for the scale filtering technique that we use here.

Figure 2 shows scalograms of the terms that describe conversion of energy between different forms. The conversion of fluid kinetic

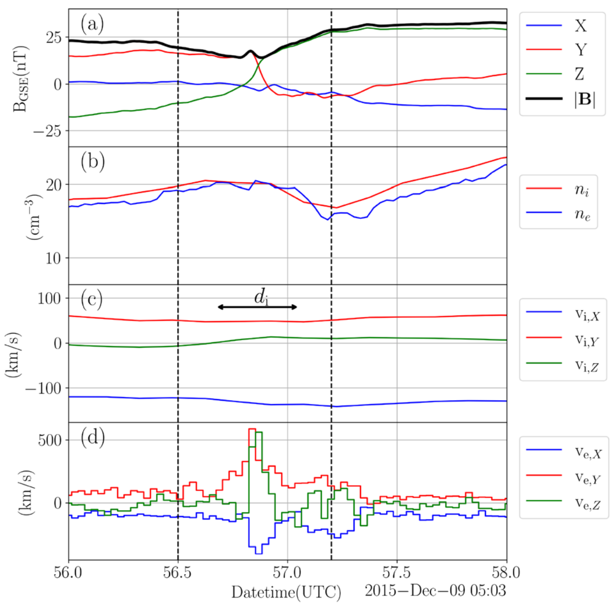

FIG. 1. Overview of the reconnection event.[37] Panel (a) shows the magnetic field components in GSE coordinates. Panel (b) shows the ion and electron densities. Panels (c) and (d) show the ion and electron velocities, respectively. The ion inertial scale d_i is indicated in panel (c).

energy into thermal energy is denoted by $PS^<_\alpha$, and electromagnetic energy is denoted by $W^<_\alpha$ and vice versa. Positive values of these quantities indicate a conversion from bulk flow energy at large scales to either thermal or electromagnetic energy. The first three panels show the dissipation (as measured by $PS^<_\alpha$) occurring on ions and electrons as well as the total dissipation. We observe that the dissipation due to both ions and electrons starts increasing rapidly as the filtering scale becomes smaller than the ion kinetic scales, indicating that the conversion from the bulk flow energy to the thermal energy occurs predominantly at sub-ion scales. A similar trend is observed in the last three panels of Fig. 2, which show the conversion of the bulk flow energy into electromagnetic energy also onsets at sub-ion scales. However, the electromagnetic work performed on the ions is significantly smaller than that for electrons.

A notable feature is that opposite polarity of thermal energy conversion, respectively, corresponding to heating and cooling are observed on the two sides of the current sheet [panels (a) and (b)]. One possible explanation is that this is associated with the properties of guide field reconnection. In strong guide field reconnection, there is a strong thermal pressure along one of the separatrix, along which there exists a high velocity shear. As a result, the pressure–strain interaction (dominated by Pi-D) is strong and positive along this separatrix, suggesting that the flow energy is converted to thermal energy. Along the other separatrix, pressure–strain interaction is weak, and therefore, a cooling effect is observed.

Figure 3 shows the terms responsible for transferring energies of a given form across scales, without any change in the form [first terms on the right hand side of Eqs. (7) and (8)]. From the first three panels, it is clear that the majority of the kinetic energy flux is carried by the electron fluid, and they become dominant at sub-ion scales. There is a

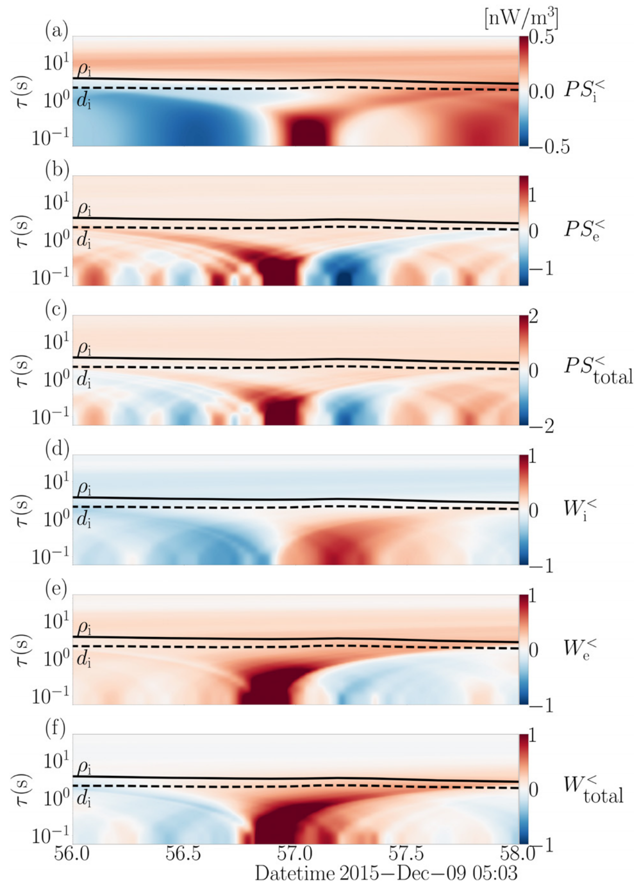

FIG. 2. Energy conversion between different forms in a magnetic reconnection region. Panels (a) and (b) show the pressure–strain interaction on ions and electrons as a function of the filtering timescale. The total (ion+electron) dissipation is shown in panel (c) as $PS^<_{\text{total}} = \sum_\alpha PS^<_\alpha$. Panels (d) and (e) show the filtered contribution to the electromagnetic work ($\mathbf{j}.\mathbf{E}$) from ions and electrons, respectively. Panel (f) shows the total electromagnetic work, $W^<_{\text{total}} = \sum_\alpha W^<_\alpha$ as a function of the filtering timescale. The ion gyroradius ρ_i and the Taylor-shifted ion inertial length d_i are shown in each panel using the solid and dotted black lines, respectively.

minor contribution by the ion fluid (Π^{uu}_i) at large scales. The electromagnetic energy too plays a minor role in the total energy flux, as was found previously in simulations of turbulence as well.[3,40] The sub-ion cascade of energy at reconnection regions was recently reported by Manzini *et al.*,[10] but this work identifies the separate components. Similar to energy conversion, two opposite directions in flux are seen on the two sides of the current sheet [panels (b), (c), and (e)].

IV. KINETIC SIMULATIONS

We use a kinetic particle-in-cell (PIC) simulation of a 2.5D magnetic reconnection performed using the p3d code.[41] In this setup, all vector fields have three components with only in-plane fluctuation gradients; there is no variation along the z (out-of-plane) direction. The system uses a particular set of normalizations, where the number density and magnetic field are normalized to some reference values n_0 and B_0, respectively. Mass is normalized to ion mass m_i, length is

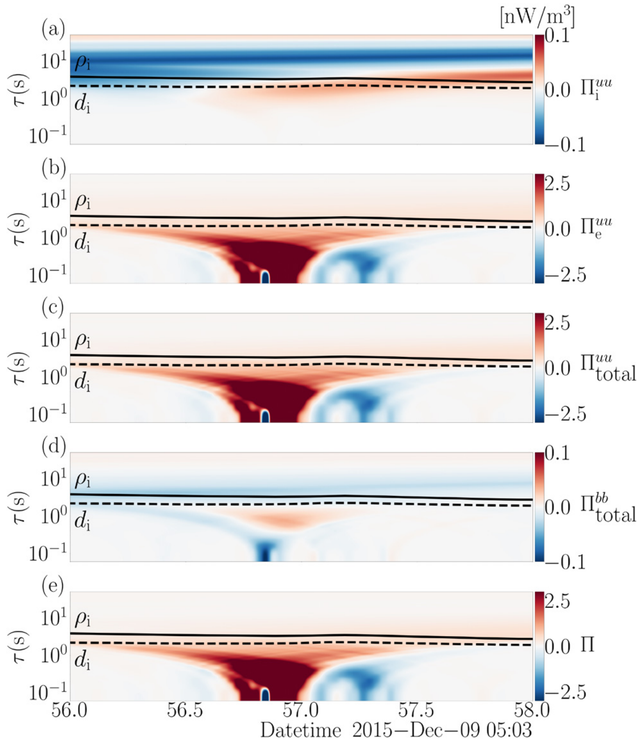

FIG. 3. Energy flux of different energy forms in a magnetic reconnection region. Panels (a) and (b) show the flux of the ion kinetic energy and electron kinetic energy as a function of the filtering timescale. Panel (c) shows the total kinetic energy flux, $\Pi^{uu}_{\text{total}} = \sum_\alpha \Pi^{uu}_\alpha$, across scales. Panel (d) shows the electromagnetic energy flux across scales ($\Pi^{bb}_{\text{total}} = \sum_\alpha \Pi^{bb}_\alpha$), and panel (e) shows the total energy flux (electromagnetic + kinetic) across scales ($\Pi = \sum_\alpha \Pi^{uu}_\alpha + \Pi^{bb}_\alpha$). The ion gyroradius ρ_i and the Taylor-shifted ion inertial length d_i are shown in each panel using the solid and dotted black lines, respectively.

normalized to the ion inertial length $d_i = \sqrt{m_i c^2/4\pi n_0 e^2}$, time is normalized to the inverse of ion cyclotron frequency $\omega_{ci}^{-1} = (eB_0/m_i c)^{-1}$, and speed is normalized to the ion Alfvén speed $v_A = \sqrt{B_0^2/4\pi m_i n_0}$. The electric field is normalized to $E_0 = v_A B_0/c$, and the temperature is normalized to $T_0 = \frac{1}{2} m_i v_A^2$.

The simulation is initialized within a periodic domain of size $L = 204.8\, d_i$ with a double Harris equilibrium, and a sinusoidal perturbation of amplitude 0.12 is added to initiate reconnection dynamics. The system has a grid spacing of $\delta x = 0.05\, d_i$ with 4096 grids on each side and a time step of $\delta t\omega_{ci} = 0.01$ and uses 100 particles per grid with a total of 1.68×10^9 particles for each species. Additional settings are mass ratio $m_i/m_e = 25$ and the speed of light $c = 15 v_A$. The reconnecting field is $B_r = 1$, the out-of-plane guide magnetic field is $B_g = 2$, the background density is $n_b = 0.2$, and the temperature for ions and electrons is set to be $T_i = 1.25$ and $T_e = 0.25$, respectively, with a total plasma beta of $\beta = 0.12$. This simulation was previously reported in Refs. 9 and 42.

Figure 4 provides an overview of the simulation showing the out-of-plane current j_z closer to the X-line for the upper current sheet with contours of the magnetic field lines. At this time of analysis $t\omega_{ci} = 360$, reconnection is well developed as the system is in the early quasi-steady reconnection phase, and the mean square current has reached its maximum. The current sheet is shifted toward the separatrix, a signature of component reconnection.

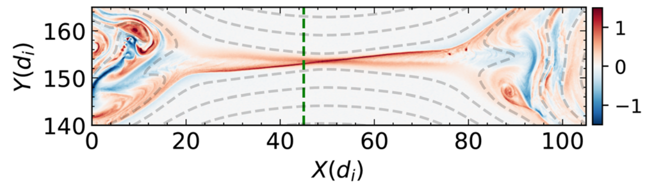

FIG. 4. Overview of the out-of-plane current j_z closer to the X-line in the upper current sheet of the reconnection simulation at $t\omega_{ci} = 360$ with contours of magnetic flux. The dashed green line represents the cut along which the analysis is performed.

For our analysis, we take a cut at $x = 45\, d_i$, shown by the vertical dashed green line in Fig. 4. At each scale, a two-dimensional boxcar filter is used to compute the terms in the filtered equations, following which a 1D cut is taken close to the X-point. The 1D cuts of the filtered quantities are computed and then vertically arranged as a 2D image, with the filtering scale on the y-axis. The resulting scalograms for the energy conversion and energy transfer terms are shown in Figs. 5 and 6. The panels in these figures follow the same order as the scalograms for the observations in Figs. 2 and 3.

Inspection of Fig. 5 indicates that both proton and electron dissipation (production of internal energy) "turn on" at scales of a few ion inertial lengths and persist toward the smaller scales for the central event near $y = 152\, d_i$ to $153\, d_i$. This is qualitatively similar to the pattern of dissipation near the reconnection event in Fig. 2 in that both occur near the ion kinetic scales and persist at smaller scales.

For the electrons, a phase of significant cooling just offset in space at $y \approx 154\, d_i$ is seen in the simulation, in panel (b) of Fig. 5. A similar cooling feature is observed in the electron dissipation in the MMS observations in Fig. 2. However, the overall heating dominates, and again the onset is around d_i and persisting at smaller scales. The filtered electromagnetic work for the simulation analysis is shown in panels (d)–(f) of Fig. 5. These also show a very strong feature centered on the current sheet crossing as described in Fig. 4. The width of the enhanced electromagnetic energy conversion is noticeably wider than the spatial span of the filtered dissipation *PS* in panels (a)–(c). Similar behavior is seen in the MMS observations (Fig. 2). Like the filtered pressure strain, the filtered electromagnetic work is also turning on at scales near but somewhat larger than d_i in the simulation.

The scalogram analysis of cross-scale energy fluxes for the PIC simulation is shown in Fig. 6, in analogy to the MMS analysis in Fig. 3. From panels (a) and (b), we observe that the proton energy flux is, in general, weaker than the electron energy flux, though both turn on at a scale of about $5\, d_i$, and over a region spanning 3–5 d_i centered around the reconnecting current sheet. There is a region of fairly strong inverse energy flux in the electron channel offset by about $1\, d_i$ toward the larger y direction. The total energy flux [panel (c)] has nearly identical appearance to the electron energy flux, confirming that the proton energy flux is generally much weaker. It is interesting to note that the general morphology of the energy flux in electrons is similar in the simulations [panel (b) of Fig. 6] and in the MMS observations [panel (b) of Fig. 3]. For the simulations, panel (d) shows the electromagnetic energy flux, which similarly turns on at a few d_i near the current sheet,

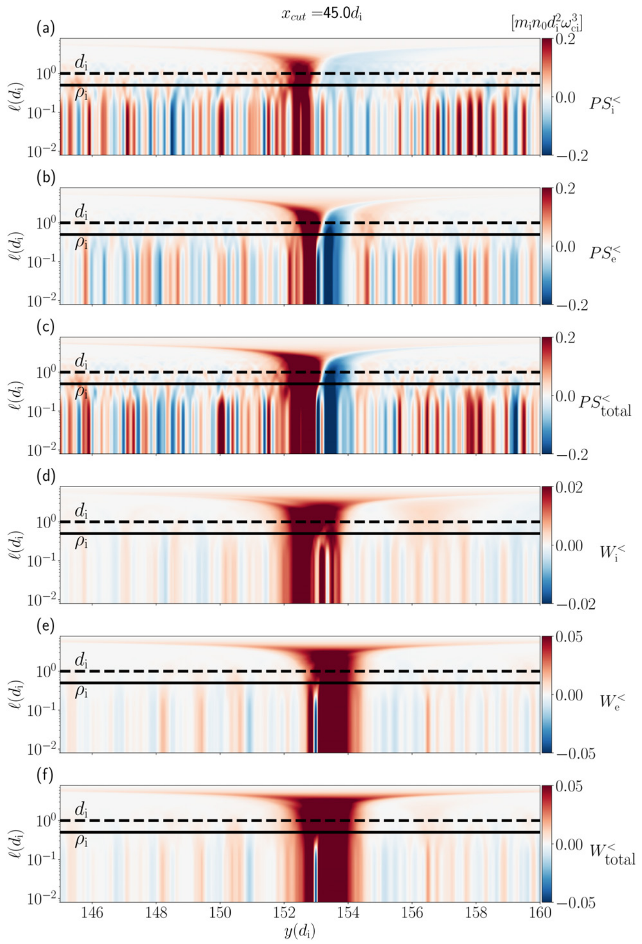

FIG. 5. Analysis of energy conversion in the simulation. The panels follow the same order as in Fig. 2. Panels (a) and (b) show the pressure-strain interaction on ions and electrons as a function of scale. Panel (c) shows the total dissipation as a function of scale, given by $PS^<_{\mathrm{total}} = \sum_\alpha PS^<_\alpha$. Panels (d) and (e) show the filtered contribution to the electromagnetic work on ions and electrons, respectively. Panel (f) shows the total electromagnetic work, $W^<_{\mathrm{total}} = \sum_\alpha W^<_\alpha$, as a function of scale. The ion gyroradius ρ_i and the ion inertial length d_i are shown in each panel using the solid and dotted black lines, respectively. The ion gyroradius is calculated using the total magnetic field (reconnecting and guide field).

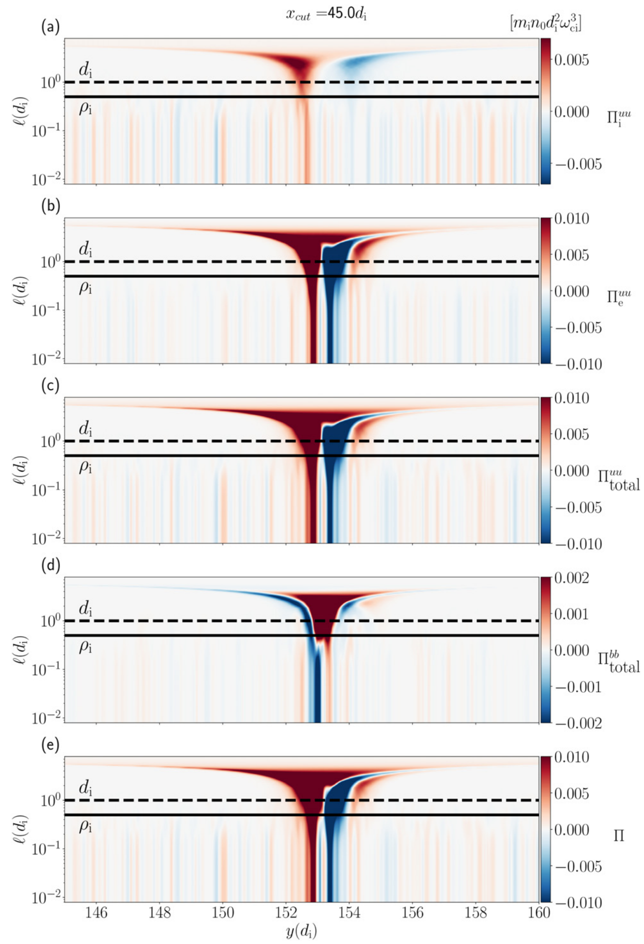

FIG. 6. Analysis of cross-scale energy fluxes in the simulation. The panels follow the same order as in Fig. 3. Panels (a) and (b) show the flux of the ion kinetic energy as a function of scale. Panel (c) shows the total flux of the kinetic energy across scales ($\Pi^{uu}_{\mathrm{total}} = \sum_\alpha \Pi^{uu}_\alpha$). Panel (d) shows the total flux of the electromagnetic energy across scales ($\Pi^{bb}_{\mathrm{total}} = \sum_\alpha \Pi^{bb}_\alpha$), and panel (e) shows the total energy flux (electromagnetic + kinetic) across scales ($\Pi = \sum_\alpha \Pi^{uu}_\alpha + \Pi^{bb}_\alpha$).

and is attenuated sharply at scales smaller than about $d_i/2$. A narrow region of inverse transfer precedes the current sheet by a small distance (less than 1 d_i). The weak oscillations preceding and following the current sheet crossing in Figs. 5 and 6 are likely of little significance and are probably due to PIC noise.

A comparison of the cross-scale kinetic energy fluxes and the dissipation terms (for both ions and electrons) in the observation and the simulation is shown in Fig. 7. For the MMS event, these terms are integrated over the reconnecting current sheet, as delineated by the vertical dotted lines in Fig. 1, and for the simulation, the integration limits are from 151 to 155 d_i. In both observations and simulations, we observe that both the ion and electron dissipation terms ($PS^<_\mathrm{i}$ and $PS^<_\mathrm{e}$), shown in panels (a) and (b), are quite small above the ion inertial scales and start increasing significantly as we progress toward sub-ion scales. For the kinetic energy fluxes, we can observe that the ion fluxes [panel (c)] are much smaller than that for the electrons [panel (d)], and the latter exhibit a single strong peak in the vicinity of 0.1 d_i in both cases. This behavior is somewhat similar to the one seen in classical turbulence, with fluxes becoming dominant at intermediate range and dissipation becoming dominant at small scales.

V. DISCUSSION

In this study, we investigated the scale-dependent energy transfer and conversion occurring near the reconnection X point. Our two main findings can be summarized as follows.

- First, in addition to a sub-ion cascade, reconnection triggers a sub-ion scale dissipation. The dissipation, quantified here as the pressure-strain interaction for each species, is measured here in

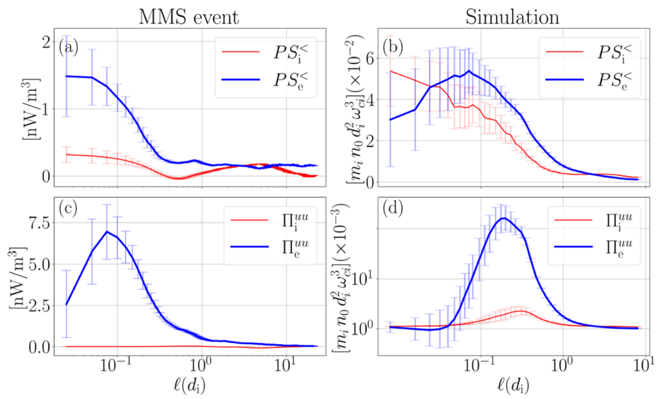

FIG. 7. Comparison of energy dissipation and flux in the MMS event and the simulation. The panels on the left show the results from the MMS observation, and the panels on the right show the same quantities plotted for the simulation. Panels (a) and (b) show the pressure–strain interaction contributions from ions and electrons as a function of scale, integrated over the reconnection region. Panels (c) and (d) show the ion and electron kinetic energy fluxes as a function of scale. The standard errors have been shown in each panel using the red error bars for ions and blue error bars for electrons.

both ion and electron channels. These become active near ion kinetic scales and remain strong at smaller scales.

- Second, the energy cascade, triggered by reconnection, is mostly carried by the electron fluid, with minor contribution from ion fluid and electromagnetic field. The ability to draw these conclusions depends on the novel analysis of reconnection presented here based on the scale filtering method.

A similar result was recently obtained by Manzini *et al.*[10] and Foldes *et al.*[22] However, we find additionally that the flux of the electron kinetic energy Π_e^{uu} dominates below ion kinetic scales and is almost two orders of magnitude higher in the MMS event. In the simulation, however, we find that the electron energy flux is only about 2 times larger than the ion energy flux instead of being about 50 times larger as found in the observations. This could possibly be attributed to the artificial mass ratio $m_i/m_e = 25$ used in the simulation.[43] The observation of the enhanced electron energy flux stands in contrast to results found in simulations of reconnection,[9] where the total energy flux was found to peak at scales above the ion inertial scale.

The key distinction between the observational analysis and the analysis used in the simulations was that the simulations used global averages of the energy fluxes, which dilutes/smooths out the local enhancements of the energy fluxes occurring close to the X-point, while with MMS, the scalograms clearly illustrate these local enhancements. This points to reconnection sites as a manifestation of intermittency in larger turbulence systems. Producing scalograms of the energy fluxes in the simulations, we find a qualitative agreement between observations and simulations.

There is, however, a discrepancy between the MMS observations and the simulation regarding the scale at which the dissipation (pressure strain) and energy fluxes turn on. For the MMS analysis, these turn on at or below the ion inertial scale d_i. For the simulation, both turn on at scales somewhat larger than d_i. One possible explanation lies in the higher degree of compressional activity anticipated in the magnetosheath, whereas standard PIC simulations such as that analyzed here are relatively incompressible. Recent work on pressure-strain[44] shows that *PiD* (the anisotropic part of the pressure–strain interaction) also has a compressive element to it and is often anticorrelated with the pressure dilatation. It is unknown whether this effect and the lower level of compressions in the simulation might alter the scale at which these documented effects turn on. If one could estimate the incompressive contribution to pressure strain, then it would shed light on the role of incompressive heating at those lag scales. This cannot be examined in analysis of MMS data, since a Helmholtz decomposition cannot be done with only four spacecraft. Such a determination would require significant additional PIC simulation and analysis.

It is also worthwhile to note that we observe the simultaneous presence of a direct and an inverse transfer of the kinetic and the electromagnetic energies in the simulation (in Fig. 6), and to a lesser extent, in the MMS data (in Fig. 3). We recall that in a standard Kolmogorov cascade, the underlying sea of triadic interactions consists of both large-to-small (direct) transfer and small-to-large (inverse) transfer, the former being dominant in the direct cascade scenario.[45] Usually, the identification of an inverse cascade would require sampling a statistically significant volume of the turbulence. Here, due to the observation of transfer across scales locally in real space, we have an opportunity to observe a dominant direct transfer near the current sheet and a region of inverse transfer nearby. It is unclear whether such nonuniformity of the transfer might be related to a change in the type of cascade.[46,47] It is known from prior studies that kinetic effects near reconnecting current sheets can exhibit strong gradients. Quantities such as temperature anisotropy, pressure strain, and electromagnetic work can show regional correlations, including sign reversals due to small-scale features that form near a central current sheet. This is seen, for example, in Refs. 28 and 48. In this sense, it is not unexpected that energy flux would show such regional complexity.

We should also note that the transport terms could potentially play an important role in the energy balance in observations, since unlike in a periodic simulation domain, these terms will likely not vanish in a realistic turbulent domain such as the Earth's magnetosheath.[49]

ACKNOWLEDGMENTS

This research was supported in part by the NASA Heliospheric GI under Grant No. 80NSSC21K0739 and NASA under Grant No. 80NSSC21K1458 at Princeton University, and Subcontract No. SUB0000317 to Delaware; the MMS Theory and Modeling under Grant No. 80NSSC19K0565 at Delaware; and the NSFDOE under Grant No. PHYS-2108834 at Delaware. The authors acknowledge the Texas Advanced Computing Center (TACC) for providing resources that have contributed to the research results reported within this paper. The authors also acknowledge high-performance computing support from Cheyenne (doi:10.5065/D6RX99HX) and Derecho (https://doi.org/10.5065/qx9a-pg09) provided by NCAR's Computational and Information Systems Laboratory, sponsored by the National Science Foundation. We thank the MMS SDC, FPI, and FIELDS teams for their assistance with this study.

AUTHOR DECLARATIONS

Conflict of Interest

The authors have no conflicts to disclose.

Version of record at: https://doi.org/10.1063/5.0278907

Author Contributions

S. Roy: Conceptualization (equal); Formal analysis (equal); Investigation (equal); Methodology (equal); Writing – original draft (equal); Writing – review & editing (equal). **R. Bandyopadhyay:** Conceptualization (equal); Funding acquisition (equal); Investigation (equal); Methodology (equal); Supervision (equal); Writing – original draft (equal); Writing – review & editing (equal). **S. Adhikari:** Formal analysis (equal); Investigation (equal); Methodology (equal); Writing – original draft (equal); Writing – review & editing (equal). **Y. Yang:** Conceptualization (equal); Formal analysis (equal); Funding acquisition (equal); Investigation (equal); Methodology (equal); Supervision (equal); Writing – original draft (equal); Writing – review & editing (equal). **W. H. Matthaeus:** Conceptualization (equal); Formal analysis (equal); Funding acquisition (equal); Investigation (equal); Methodology (equal); Supervision (equal); Writing – original draft (equal); Writing – review & editing (equal).

DATA AVAILABILITY

The data that support the findings of this study are openly available in MMS at https://lasp.colorado.edu/MMS/sdc, Refs. 50–52 and in Github at https://github.com/sohom-ud/MMS_codes.git, Ref. 53.

APPENDIX: BAROPYCNAL WORK

Here, we discuss one of the discrepancies between the two versions of the dissipation as described in Refs. 30 and 35. The differences arise due to the presence of a term known as the baropycnal work, which describes a different channel of energy transfer due to density variations in the flow. The baropycnal work is defined as $\Lambda_\ell^\alpha = (\nabla \cdot \overline{\mathbf{P}}_\alpha) \cdot (\widetilde{\mathbf{u}}_\alpha - \overline{\mathbf{u}}_\alpha)$. Taking a dot product of the divergence of the pressure tensor, $\nabla \cdot \overline{\mathbf{P}}_\alpha$, from the filtered momentum equation with the Favre filtered velocity, $\widetilde{\mathbf{u}}_\alpha$, we get $(\nabla \cdot \overline{\mathbf{P}}_\alpha) \cdot \widetilde{\mathbf{u}}_\alpha$. This term can be recast in two different ways:

1. $(\nabla \cdot \overline{\mathbf{P}}_\alpha) \cdot \widetilde{\mathbf{u}}_\alpha = \nabla \cdot (\overline{\mathbf{P}}_\alpha \cdot \widetilde{\mathbf{u}}_\alpha) - (\overline{\mathbf{P}}_\alpha \cdot \nabla) \cdot \widetilde{\mathbf{u}}_\alpha$. This is the expression we find in Ref. 35.
2. $(\nabla \cdot \overline{\mathbf{P}}_\alpha) \cdot \widetilde{\mathbf{u}}_\alpha = \nabla \cdot (\overline{\mathbf{P}}_\alpha \cdot \overline{\mathbf{u}}_\alpha) - (\overline{\mathbf{P}}_\alpha \cdot \nabla) \cdot \overline{\mathbf{u}}_\alpha + (\nabla \cdot \overline{\mathbf{P}}_\alpha) \cdot (\widetilde{\mathbf{u}}_\alpha - \overline{\mathbf{u}}_\alpha)$

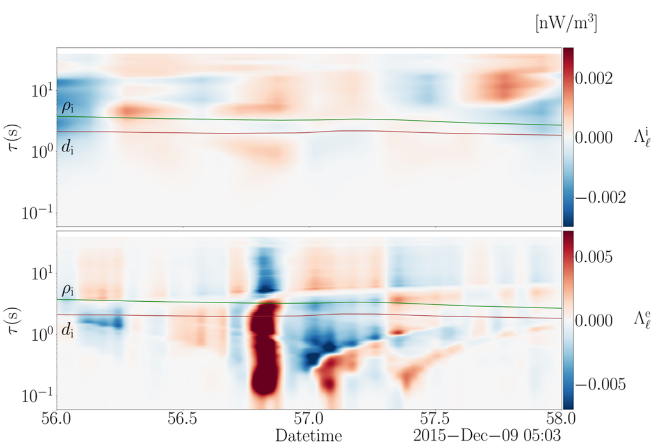

FIG. 8. Baropycnal work for ions and electrons for the MMS reconnection event.

The last term on the RHS in Eq. (2) is precisely the baropycnal work that we find in Ref. 30. As we show in Fig. 8, this term is found to be at least an order of magnitude smaller than the flux and the dissipation terms shown above for the MMS reconnection event.

REFERENCES

[1] A. N. Kolmogorov, "Local structure of turbulence in an incompressible viscous fluid at very high Reynolds numbers," Dokl. Akad. Nauk SSSR **30**, 301–305 (1941). [Reprinted in Proc. R. Soc. London, Ser. A **434**, 9–13 (1991)].
[2] D. Biskamp, *Magnetohydrodynamic Turbulence* (Cambridge University Press, 2003).
[3] W. H. Matthaeus, Y. Yang, M. Wan, T. N. Parashar, R. Bandyopadhyay, A. Chasapis, O. Pezzi, and F. Valentini, "Pathways to dissipation in weakly collisional plasmas," Astrophys. J. **891**, 101 (2020).
[4] H. Karimabadi, V. Roytershteyn, M. Wan, W. H. Matthaeus, W. Daughton, P. Wu, M. Shay, B. Loring, J. Borovsky, E. Leonardis, S. C. Chapman, and T. K. M. Nakamura, "Coherent structures, intermittent turbulence, and dissipation in high-temperature plasmas," Phys. Plasmas **20**, 012303 (2013).
[5] M. K. Verma, A. Ayyer, and A. V. Chandra, "Energy transfers and locality in magnetohydrodynamic turbulence," Phys. Plasmas **12**, 082307 (2005).
[6] A. Alexakis, P. D. Mininni, and A. Pouquet, "Shell-to-shell energy transfer in magnetohydrodynamics. I. Steady state turbulence," Phys. Rev. E **72**, 046301 (2005).
[7] H. Aluie, "Scale decomposition in compressible turbulence," Physica D **247**, 54–65 (2013).
[8] Y. Yang, W. H. Matthaeus, T. N. Parashar, C. C. Haggerty, V. Roytershteyn, W. Daughton, M. Wan, Y. Shi, and S. Chen, "Energy transfer, pressure tensor, and heating of kinetic plasma," Phys. Plasmas **24**, 072306 (2017), arXiv:1705.02054 [physics.plasm-ph].
[9] S. Adhikari, Y. Yang, W. H. Matthaeus, P. A. Cassak, T. N. Parashar, and M. A. Shay, "Scale filtering analysis of kinetic reconnection and its associated turbulence," Phys. Plasmas **31**, 020701 (2024).
[10] D. Manzini, F. Sahraoui, and F. Califano, "Subion-scale turbulence driven by magnetic reconnection," Phys. Rev. Lett. **130**, 205201 (2023).
[11] Y.-M. Huang and A. Bhattacharjee, "Turbulent magnetohydrodynamic reconnection mediated by the plasmoid instability," Astrophys. J. **818**, 20 (2016).
[12] S. Servidio, W. H. Matthaeus, M. A. Shay, P. Dmitruk, P. A. Cassak, and M. Wan, "Statistics of magnetic reconnection in two-dimensional magnetohydrodynamic turbulence," Phys. Plasmas **17**, 032315 (2010).
[13] A. Mallet, A. A. Schekochihin, and B. D. Chandran, "Disruption of Alfvénic turbulence by magnetic reconnection in a collisionless plasma," J. Plasma Phys. **83**, 905830609 (2017).
[14] A. Mallet, A. Schekochihin, and B. D. Chandran, "Disruption of sheet-like structures in Alfvénic turbulence by magnetic reconnection," Mon. Not. R. Astron. Soc. **468**, 4862–4871 (2017).
[15] W. Matthaeus and S. L. Lamkin, "Turbulent magnetic reconnection," Phys. Fluids **29**, 2513–2534 (1986).
[16] N. F. Loureiro and S. Boldyrev, "Collisionless reconnection in magnetohydrodynamic and kinetic turbulence," Astrophys. J. **850**, 182 (2017).
[17] N. F. Loureiro and S. Boldyrev, "Role of magnetic reconnection in magnetohydrodynamic turbulence," Phys. Rev. Lett. **118**, 245101 (2017).
[18] S. Adhikari, T. Parashar, M. Shay, W. Matthaeus, P. Pyakurel, S. Fordin, J. Stawarz, and J. Eastwood, "Energy transfer in reconnection and turbulence," Phys. Rev. E **104**, 065206 (2021).
[19] J. E. Stawarz, P. Muñoz, N. Bessho, R. Bandyopadhyay, T. Nakamura, S. Eriksson, D. B. Graham, J. Büchner, A. Chasapis, J. Drake *et al.*, "The interplay between collisionless magnetic reconnection and turbulence," Space Sci. Rev. **220**, 90 (2024).
[20] O. Alexandrova, V. Carbone, P. Veltri, and L. Sorriso-Valvo, "Small-scale energy cascade of the solar wind turbulence," Astrophys. J. **674**, 1153 (2008).
[21] L. Franci, S. S. Cerri, F. Califano, S. Landi, E. Papini, A. Verdini, L. Matteini, F. Jenko, and P. Hellinger, "Magnetic reconnection as a driver for a sub-ion-scale cascade in plasma turbulence," Astrophys. J. Lett. **850**, L16 (2017).
[22] R. Foldes, S. S. Cerri, R. Marino, and E. Camporeale, "Evidence of dual energy transfer driven by magnetic reconnection at subion scales," Phys. Rev. E **110**, 055207 (2024).

[23] R. Bandyopadhyay, A. Chasapis, W. H. Matthaeus, T. N. Parashar, C. C. Haggerty, M. A. Shay, D. J. Gershman, B. L. Giles, and J. L. Burch, "Energy dissipation in turbulent reconnection," Phys. Plasmas **28**, 112305 (2021).

[24] S. S. Cerri and F. Califano, "Reconnection and small-scale fields in 2D-3V hybrid-kinetic driven turbulence simulations," New J. Phys. **19**, 025007 (2017).

[25] S. Zenitani, M. Hesse, A. Klimas, and M. Kuznetsova, "New measure of the dissipation region in collisionless magnetic reconnection," Phys. Rev. Lett. **106**, 195003 (2011).

[26] R. Numata and N. Loureiro, "Ion and electron heating during magnetic reconnection in weakly collisional plasmas," J. Plasma Phys. **81**, 305810201 (2015).

[27] N. Loureiro, A. Schekochihin, and A. Zocco, "Fast collisionless reconnection and electron heating in strongly magnetized plasmas," Phys. Rev. Lett. **111**, 025002 (2013).

[28] A. Greco, F. Valentini, S. Servidio, and W. H. Matthaeus, "Inhomogeneous kinetic effects related to intermittent magnetic discontinuities," Phys. Rev. E **86**, 066405 (2012).

[29] O. Pezzi, H. Liang, J. L. Juno, P. A. Cassak, C. L. Vásconez, L. Sorriso-Valvo, D. Perrone, S. Servidio, V. Roytershteyn, J. M. TenBarge, and W. H. Matthaeus, "Dissipation measures in weakly collisional plasmas," Mon. Not. R. Astron. Soc. **505**, 4857–4873 (2021).

[30] D. Manzini, F. Sahraoui, and F. Califano, "Cascade-dissipation balance in astrophysical plasmas: Insights from the terrestrial magnetosheath," Phys. Rev. Lett. **132**, 235201 (2024).

[31] M. Germano, "Turbulence: The filtering approach," J. Fluid Mech. **238**, 325–336 (1992).

[32] G. L. Eyink, "Locality of turbulent cascades," Physica D **207**, 91–116 (2005).

[33] G. I. Taylor, "The spectrum of turbulence," Proc. R Soc. London, Ser. A **164**, 476–490 (1938).

[34] A. Favre, "Statistical equations of turbulent gases," *Problems of Hydrodynamics and Continuum Mechanics* (SIAM, Philadelphia, 1969), pp. 231–266.

[35] Y. Yang, W. H. Matthaeus, S. Roy, V. Roytershteyn, T. N. Parashar, R. Bandyopadhyay, and M. Wan, "Pressure–strain interaction as the energy dissipation estimate in collisionless plasma," Astrophys. J. **929**, 142 (2022).

[36] G. Arrò, F. Califano, and G. Lapenta, "Spectral properties and energy transfer at kinetic scales in collisionless plasma turbulence," Astron. Astrophys. **668**, A33 (2022).

[37] F. Wilder, R. Ergun, S. Eriksson, T. Phan, J. Burch, N. Ahmadi, K. Goodrich, D. Newman, K. Trattner, R. Torbert *et al.*, "Multipoint measurements of the electron jet of symmetric magnetic reconnection with a moderate guide field," Phys. Rev. Lett. **118**, 265101 (2017).

[38] J. L. Burch and T. D. Phan, "Magnetic reconnection at the dayside magnetopause: Advances with MMS," Geophys. Res. Lett. **43**, 8327–8338, https://doi.org/10.1002/2016GL069787 (2016).

[39] C. T. Russell, "Geophysical coordinate transformations," Cosmic Electrodyn. **2**, 184–196 (1971).

[40] Y. Yang, W. H. Matthaeus, T. N. Parashar, P. Wu, M. Wan, Y. Shi, S. Chen, V. Roytershteyn, and W. Daughton, "Energy transfer channels and turbulence cascade in Vlasov-Maxwell turbulence," Phys. Rev. E **95**, 061201 (2017).

[41] A. Zeiler, D. Biskamp, J. F. Drake, B. N. Rogers, M. A. Shay, and M. Scholer, "Three-dimensional particle simulations of collisionless magnetic reconnection," J. Geophys. Res. **107**, 1230, https://doi.org/10.1029/2001JA000287 (2002).

[42] S. Adhikari, M. Shay, T. Parashar, W. Matthaeus, P. Pyakurel, J. Stawarz, and J. Eastwood, "Effect of a guide field on the turbulence like properties of magnetic reconnection," Phys. Plasmas **30**, 082904 (2023).

[43] J. Edyvean, T. N. Parashar, T. Simpson, J. Juno, G. L. Delzanno, F. Guo, O. Koshkarov, W. H. Matthaeus, M. Shay, and Y. Yang, "Scale separation effects on simulations of plasma turbulence," Astrophys. J. **972**, 173 (2024).

[44] S. Adhikari, Y. Yang, and W. H. Matthaeus, "Revisiting compressible and incompressible pressure-strain interaction in kinetic plasma turbulence," arXiv:2503.11825 [physics.plasm-ph] (2025).

[45] M. K. Verma, *Energy Transfers in Fluid Flows: Multiscale and Spectral Perspectives* (Cambridge University Press, 2019).

[46] A. Alexakis, P. D. Mininni, and A. Pouquet, "Turbulent cascades, transfer, and scale interactions in magnetohydrodynamics," New J. Phys. **9**, 298 (2007).

[47] G. Sahoo, A. Alexakis, and L. Biferale, "Discontinuous transition from direct to inverse cascade in three-dimensional turbulence," Phys. Rev. Lett. **118**, 164501 (2017).

[48] T. N. Parashar and W. H. Matthaeus, "Propinquity of current and vortex structures: Effects on collisionless plasma heating," Astrophys. J. **832**, 57 (2016).

[49] S. Fadanelli, B. Lavraud, F. Califano, G. Cozzani, F. Finelli, and M. Sisti, "Energy conversions associated with magnetic reconnection," J. Geophys. Res. **126**, e2020JA028333, https://doi.org/10.1029/2020JA028333 (2021).

[50] J. L. Burch, T. E. Moore, R. B. Torbert, and B. L. Giles, "Magnetospheric multiscale overview and science objectives," Space Sci. Rev. **199**, 5–21 (2016).

[51] C. T. Russell, B. J. Anderson, W. Baumjohann, K. R. Bromund, D. Dearborn, D. Fischer, G. Le, H. K. Leinweber, D. Leneman, W. Magnes, J. D. Means, M. B. Moldwin, R. Nakamura, D. Pierce, F. Plaschke, K. M. Rowe, J. A. Slavin, R. J. Strangeway, R. Torbert, C. Hagen, I. Jernej, A. Valavanoglou, and I. Richter, "The magnetospheric multiscale magnetometers," Space Sci. Rev. **199**, 189–256 (2016).

[52] C. Pollock, T. Moore, A. Jacques, J. Burch, U. Gliese, Y. Saito, T. Omoto, L. Avanov, A. Barrie, V. Coffey, J. Dorelli, D. Gershman, B. Giles, T. Rosnack, C. Salo, S. Yokota, M. Adrian, C. Aoustin, C. Auletti, S. Aung, V. Bigio, N. Cao, M. Chandler, D. Chornay, K. Christian, G. Clark, G. Collinson, T. Corris, A. De Los Santos, R. Devlin, T. Diaz, T. Dickerson, C. Dickson, A. Diekmann, F. Diggs, C. Duncan, A. Figueroa-Vinas, C. Firman, M. Freeman, N. Galassi, K. Garcia, G. Goodhart, D. Guererro, J. Hageman, J. Hanley, E. Hemminger, M. Holland, M. Hutchins, T. James, W. Jones, S. Kreisler, J. Kujawski, V. Lavu, J. Lobell, E. LeCompte, A. Lukemire, E. MacDonald, A. Mariano, T. Mukai, K. Narayanan, Q. Nguyan, M. Onizuka, W. Paterson, S. Persyn, B. Piepgrass, F. Cheney, A. Rager, T. Raghuram, A. Ramil, L. Reichenthal, H. Rodriguez, J. Rouzaud, A. Rucker, Y. Saito, M. Samara, J.-A. Sauvaud, D. Schuster, M. Shappirio, K. Shelton, D. Sher, D. Smith, K. Smith, S. Smith, D. Steinfeld, R. Szymkiewicz, K. Tanimoto, J. Taylor, C. Tucker, K. Tull, A. Uhl, J. Vloet, P. Walpole, S. Weidner, D. White, G. Winkert, P.-S. Yeh, and M. Zeuch, "Fast plasma investigation for magnetospheric multiscale," Space Sci. Rev. **199**, 331–406 (2016).

[53] R. Sohom Roy (2025). "Collection of scripts to analyze MMS data," Github, Dataset. https://github.com/sohomud/MMS_codes.git